Effect of Ba incorporation on pressure-induced structural changes in the relaxor ferroelectric PbSc$_{0.5}$Ta$_{0.5}$O$_3$

A.-M. Welsch,[1] B. J. Maier,[1] J. M. Engel,[2] B. Mihailova,[1,*,†] R. J. Angel,[3,*,‡] C. Paulmann,[1] M. Gospodinov,[4]
A. Friedrich,[5] R. Stosch,[6] B. Güttler,[6] D. Petrova,[7] and U. Bismayer[1]

[1]*Mineralogisch-Petrographisches Institut, Universität Hamburg, Grindelallee 48, 20146 Hamburg, Germany*
[2]*Institut für Werkstoffwissenschaften, Technische Universität Dresden, Helmholtzstr. 7, 01069 Dresden, Germany*
[3]*Virginia Tech Crystallography Laboratory, Department of Geosciences, Virginia Tech, Blacksburg, Virginia 24060, USA*
[4]*Institute of Solid State Physics, Bulgarian Academy of Sciences, Boulevard Tzarigradsko Chausse 72, 1784 Sofia, Bulgaria*
[5]*Institut für Geowissenschaften, Goethe-Universität Frankfurt, Altenhöferallee 1, 60438 Frankfurt am Main, Germany*
[6]*Physikalisch-Technische Bundesanstalt, Bundesallee 100, 38116 Braunschweig, Germany*
[7]*South-West University "Neofit Rilski," 66 Ivan Mihailov str., 2700 Blagoevgrad, Bulgaria*
(Received 9 June 2009; revised manuscript received 3 August 2009; published 28 September 2009)

Pressure-induced structural changes in the canonical relaxor Pb$_{0.78}$Ba$_{0.22}$Sc$_{0.5}$Ta$_{0.5}$O$_3$ were studied with both in-house and synchrotron single-crystal x-ray diffraction as well as Raman spectroscopy at pressures up to 9.8 GPa. The results reveal that the substitution of Ba for Pb in ABO_3 perovskite-type structures, i.e., the substitution of a two-valent element with an isotropic electron shell for an isovalent element with a stereochemically active lone pair, leads to a "diffuse pressure-induced phase transition," a structural transformation over a broad pressure range, without a well-defined critical pressure point. The smeared phase transition of the average structure results from the existence of local structural deformations in the vicinity of A-positioned Ba cations.

I. INTRODUCTION

The challenge to optimize the functionality of advanced materials by tuning their nanoscale atomic arrangements has provoked considerable scientific efforts into the design and structural characterization of novel materials. Lead-based perovskite-type (ABO_3) relaxors form a special class of ferroelectric materials which show extremely large dielectric permittivity, electroelastic and electro-optic coefficients that have therefore been identified as a possible new generation of materials for information storage and processing.[1] Their unique relaxor properties are related to the strong deviation of their local structure from the global average structure.[2] The coexistence of chemically cation-ordered and disordered spatial regions as well as polar nanoclusters of various sizes and shapes within a paraelectric matrix is typical of these relaxor structures. Polar nanoregions nucleate well above the temperature of the dielectric maximum T_m and persist at temperatures below T_m. For canonical relaxors polar nanoregions do not merge to form normal ferroelectric domains even at very low temperatures. The atomistic mechanism of the formation of relaxor state remains an open question. In particular, it is still unclear if the primary reason for the suppression of ferroelectric long-range order is the charge imbalance associated with the chemical disorder on the B-site or local strains induced by chemical A-site disorder. Recently, a new canonical relaxor Pb$_{0.78}$Ba$_{0.22}$Sc$_{0.5}$Ta$_{0.5}$O$_3$ (PST-Ba) was synthesized.[3] As-made single crystals of this compound exhibit considerably larger B-site ordered domains than those in the corresponding Ba-free counterpart PbSc$_{0.5}$Ta$_{0.5}$O$_3$ (PST), although the latter undergoes a phase transition to a normal ferroelectric state.[4] This indicates that the dilution of the Pb^{2+} system with cations showing no affinity to form lone-pair electrons plays a more important role for the relaxor behavior than the size of chemically B-site ordered regions.

Pressure is a much stronger driving force than temperature and, thus, high-pressure experiments are essential to elucidate the structural peculiarities and transformation processes in perovskite-type relaxors. However, structural analyses of relaxors at high pressure (HP) have been performed only on materials of type Pb(B',B'')O$_3$,[5–16] i.e., having merely Pb^{2+} on the A site, and on two Pb-free relaxors, Na$_{0.5}$Bi$_{0.5}$TiO$_3$ and BaTi$_{0.65}$Zr$_{0.35}$O$_3$.[5,17,18] The results obtained on all Pb-based perovskite-type relaxors indicate that above a certain characteristic pressure the ferroic ordering is increased. Our recent study on PST as a model Pb(B',B'')O$_3$ compound clearly revealed the occurrence of a pressure-induced second-order phase transition in this class of materials.[14] The phase transition involves decoupling of the off-centered Pb and B-site cations within the polar nanoregions, which allows the B cations to move back to the octahedral centers, while the coherence length of the ferroic off-centered shifts of Pb is increased.

The objective of this paper is to analyze in detail the pressure-induced structural changes in PST-Ba as a model relaxor of the type (Pb,Ba)(B',B'')O$_3$ and, thus, to better understand the effect of incorporation of cations with an isotropic outermost electron shell into a system of isovalent cations having an affinity to form stereochemically active lone pairs. The pressure evolution of the local structure of PST-Ba single crystals was studied by Raman scattering, whereas the alteration of the average structure was followed by in-house and synchrotron single-crystal x-ray diffraction (XRD).

II. EXPERIMENTAL DETAILS

Cubic-shaped PST-Ba single crystals of optical and chemical homogeneity were synthesized by the high-temperature solution growth method.[3] The HP experiments

were performed in diamond-anvil cells (DACs) on specimens of approximate size $80 \times 80 \times 40$ μm^3, cut from polished {100} plates. Stainless steel gaskets with a thickness of 250 μm, preindented to $\sim$100 μm, were used in all HP experiments. A 4:1 methanol-ethanol and a 16:3:1 methanol-ethanol-water mixture were used as pressure transmitting media in single-crystal XRD and Raman spectroscopic measurements, respectively, which ensured hydrostatic conditions up to 9.8 GPa.[19]

The pressure evolution of the unit-cell parameters was followed by in-house single-crystal XRD with a Huber four-circle diffractometer using the eight-position-centering diffraction-beam method[20] with least-squares full profile fitting of the diffraction maxima[21] followed by a constrained vector-least-squares fit of the unit-cell parameters.[22] The experiments were carried out with a DAC of ETH design.[23] Pressure was determined by measuring the unit-cell volume of a quartz crystal placed next to the sample, which allowed for the very precise determination of the equation of state (EOS).[21]

High-pressure synchrotron single-crystal XRD experiments were conducted on the F1 beamline at HASYLAB/DESY using a MarCCD 165 detector and a radiation wavelength λ=0.4000 Å. The data were collected at a sample-to-detector distance of 80 mm, with a step width of 0.5° per frame and exposure times of 120 s, using a DAC of Boehler-Almax design.[24] The raw diffraction images from the MarCCD were evaluated with the Oxford Diffraction software package CRYSALIS. The ruby-line photoluminescence method was used to determine the pressure.[25] The pressure-induced R1-line shift was measured by a DeltaNu portable Raman spectrometer.

Raman-scattering measurements were performed with a Horiba Jobin-Yvon T64000 triple-grating spectrometer using the 514.5 nm line of an Ar$^+$ laser. Samples for the HP measurements were loaded in a gas-membrane driven DAC [Diacell® μScopeDAC-RT(G), easyLab] with pressure determined by the shift of the photoluminescence peak of ruby chips included in the DAC. The Raman spectra were collected in backscattering geometry, with an Olympus BH41 microscope and a 50$\times$ long-working distance objective. A background spectrum was collected at each pressure and subsequently subtracted from the sample spectrum to eliminate any signal from the pressure medium. The background-corrected spectra were temperature reduced to account for the Bose-Einstein occupation factor. The peak positions, full widths at half maximum and integral intensities were then determined by fitting the spectrum profiles with Lorentzian functions. The repeatability of the spectral features and trends was verified on several different specimens. In all three types of experiments, the reversibility of the observed structural changes was confirmed by measurements on decompression.

III. RESULTS AND DISCUSSION

As in the case of PST,[14] no splitting of the diffraction peaks was observed by in-house single-crystal XRD. Therefore the average structure of PST-Ba was considered to be
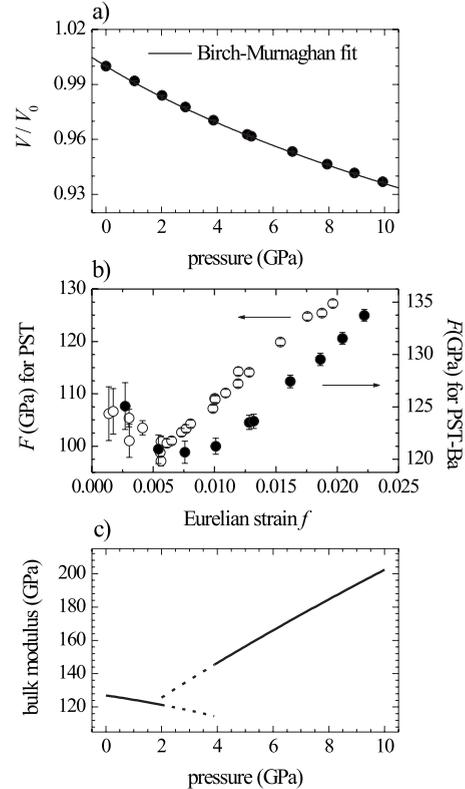

FIG. 1. (a) Pressure dependence of the pseudocubic unit-cell volume of PST-Ba normalized to the volume at ambient pressure, (b) the normalized pressure $F = p/3f(1+2f)^{5/2}$ versus the Eulerian strain $f = [(V_0/V)^{2/3} - 1]/2$ for PST-Ba (solid circles) compared with that for PST (open circles), and (c) the bulk modulus K of PST-Ba for the low- and high-pressure phase, calculated from the data below 2.0 GPa and above 3.9 GPa, respectively; the dashed lines in (c) represent the extrapolations of $K(p)$ in the range of 2.0–3.9 GPa.

pseudocubic. The symmetry of a simple cubic ABO_3 perovskite structure is $Pm\bar{3}m$ with a unit-cell parameter $a \sim 4$ Å, and this would be the symmetry of a relaxor with complete chemical disorder of the cations on the octahedral B site. XRD intensity data from PST-Ba at ambient pressure clearly revealed the existence of half-integer reflections that indicate that this sample has long-range chemical order on the B sites, and thus space group $Fm\bar{3}m$ with a doubled unit cell and $a \sim 8$ Å. Throughout this paper we will therefore refer to the $Fm\bar{3}m$ space group, when discussing Bragg reflection indices and normal phonon modes.

The pressure evolution of the normalized unit-cell volume of PST-Ba shows no exceptional behavior in the pressure range of the measurements [see Fig. 1(a)]. For PST-Ba all experimental points between ambient pressure and 10 GPa could be fit with a third-order Birch-Murnaghan EOS,[26] leading to the following values of the initial unit-cell volume, the bulk modulus and its first derivative over pressure, respectively: V_0=544.52±0.09 Å^3, K_0=110.2±1.9 GPa, and K'_0=9.9±0.6. The f-F diagram [Fig. 1(b)], in which the normalized pressure $F = p/3f(1+2f)^{5/2}$ is plotted against the Eulerian strain $f = [(V_0/V)^{2/3} - 1]/2$, indicates however that the compression behavior of the average unit cell does not fol-

low an ordinary EOS. In PST the existence of a second-order phase transition corresponds to a minimum of $F(f)$, with negative and positive values of dF/df below and above the critical pressure, respectively.[14] The f-F plot of PST-Ba and pure PST are compared in Fig. 1(b). As can be seen, a negative slope below 2.0 GPa and a positive slope above 3.9 GPa are also observed for PST-Ba. However, contrary to PST, the minimum of $F(f)$ for PST-Ba is not well defined and has a plateaulike shape between 2 and 4 GPa. The subsequent use of two different sets of EOS parameters to fit the unit-cell volume data of PST below and above the critical pressure $p_c=1.9$ GPa allowed the discontinuity in the bulk modulus at p_c to be determined.[14] Likewise, we have calculated the low-pressure bulk modulus of PST-Ba by fitting only the experimental points corresponding to the negative slope of the f-F plot, i.e., below 2.0 GPa, while the high-pressure bulk modulus of PST-Ba was obtained from the experimental points corresponding to the positive $F(f)$ slope, i.e., above 3.9 GPa [see Fig. 1(c)]. The results show that the first derivative of the low-pressure bulk modulus dK/dp is negative, which reveals structure softening, whereas the structure stiffens above 3.9 GPa with $dK/dp > 4$. In the pressure range of the plateaulike minimum between 2 and 4 GPa $dK/dp=4$, which is consistent with a second-order truncation of the Birch-Murnaghan EOS. Thus, the $F(f)$ diagram and the bulk modulus changes in PST-Ba reveal a broad, diffuse phase transition over a pressure range of 2–4 GPa, without exhibiting a distinctive critical pressure point. Therefore, the incorporation of Ba in to PST smears out the pressure-induced phase transition.

To gain further insight into the pressure-driven ordering processes in $(Pb,Ba)(B',B'')O_3$-type materials we analyzed the x-ray scattering of PST-Ba using high-energy synchrotron radiation. We collected data from the same specimen at 1.1, 2.7, 4.0, and 5.9 GPa. Figure 2 shows the $(hk0)$, $(hk1)$, and $(hk2)$ layers of the reciprocal space reconstructed from synchrotron single-crystal XRD measurements at 1.1 GPa. At this pressure the diffraction pattern resembles that at ambient conditions[4] and confirms that the low-pressure average structure of PST-Ba has $Fm\bar{3}m$ symmetry. The allowed diffraction peaks in this symmetry have Miller indices h,k,l, all even, or h,k,l, all odd. Both A- and B-site cations contribute to (hkl) diffraction peaks with $h,k,l=2n$ (n integer). The A and B cations contribute additively to the Bragg reflections with $h+k+l=4n$ and, hence, generate the stronger peaks in the $(hk0)$ and $(hk2)$ layers, whereas the two types of cations contribute in antiphase to the Bragg reflections with $h+k+l=4n+2$ and, consequently, give rise to the weaker peaks in the $(hk0)$ and $(hk2)$ layers. Only the alternating B' and B'' cations along $\langle100\rangle$ contribute to Bragg reflections with $h,k,l=2n+1$ and, therefore, such diffraction peaks in the $(hk1)$ layer are indicative of the existence of compositional 1:1 B-site order. The diffuse x-ray scattering along the $\langle110\rangle^*$ reciprocal-space directions arises from polar nanoregions comprising cation off-centered shifts that correlate within $\{110\}$ planes of the real space.[27,28] Similar to pure PST (Ref. 14) and other Pb-based relaxors,[7,11,12] pressure suppresses the x-ray diffuse scattering in PST-Ba (see Fig. 3). The diffuse x-ray scattering is already suppressed at 2.7 GPa, which
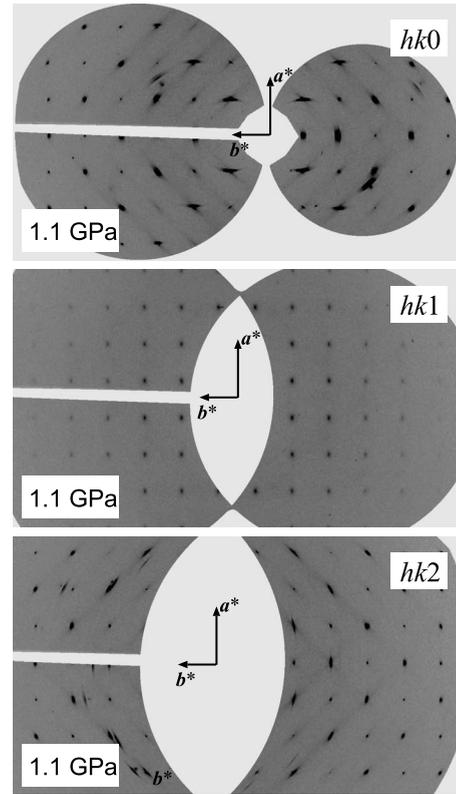

FIG. 2. Reciprocal space layers reconstructed from single-crystal synchrotron XRD measurements at 1.1 GPa.

is in the plateaulike minimum of $F(f)$ and confirms that transformation processes occur above 2 GPa, as deduced from EOS. The suppression of the diffuse scattering streaks at high pressure was explained on the basis of a HP structural analysis of PST:[14] pressure induces a long-range order of antiparallel off-centered shifts of Pb^{2+} cations accompanied by antiphase octahedral tilts and, at the same time, reduces the off-centered shifts of the B-site cations. Therefore, atomic ferroic ordering on a relatively short length scale, sufficient to produce $\langle110\rangle^*$ diffuse scattering but not "ferroelectric" Bragg reflections, vanishes at high pressures on the account of a well-developed noncubic order of the A-cation displacements, together with the suppression of the incoherent B-cation polar shifts. The resemblance between the pressure evolution of the diffuse x-ray scattering of PST and PST-Ba indicates that similar cation rearrangements take place in PST-Ba as well.

The pressure evolution of the local structure was followed by Raman spectroscopy. The trend in the overall Raman scattering is shown in Fig. 4. The observed Raman peaks were previously attributed to definite atomic vibrations on the basis of polarized spectra of lead scandium niobates and tantalates measured at ambient pressure and different temperatures.[3,4,29,30] Hence, the number of replicas used to fit the spectrum at ambient pressure is consistent with the number of expected peaks; the HP spectra were fit with the same number of Lorentzians. In an ABO_3 structure of $Fm\bar{3}m$ symmetry there are four Raman-active phonon modes: $A_{1g}+E_g+2F_{2g}$. The A_{1g} and E_g modes are related to internal sym-

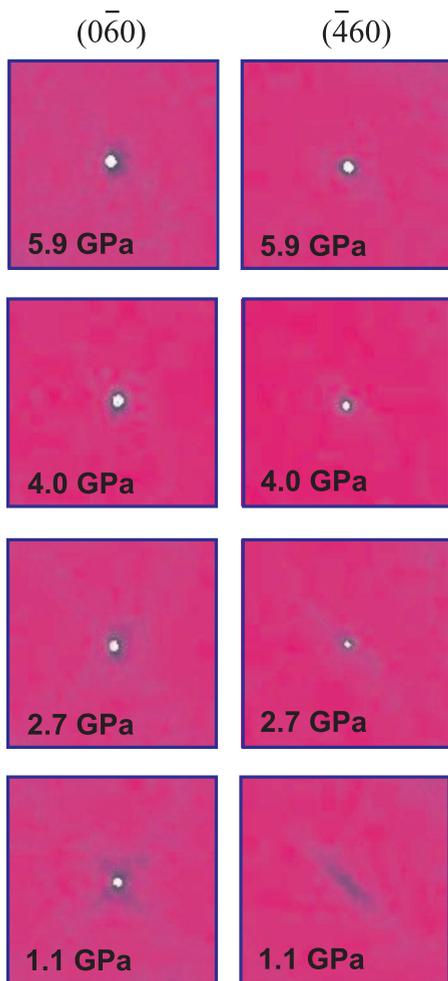$(0\bar{6}0)$ $(\bar{4}60)$

FIG. 3. (Color) Selected reciprocal space segments representing the pressure evolution of the diffuse x-ray scattering along $\langle 110 \rangle$, which is related to off-centered cation shifts in polar nanoregions.
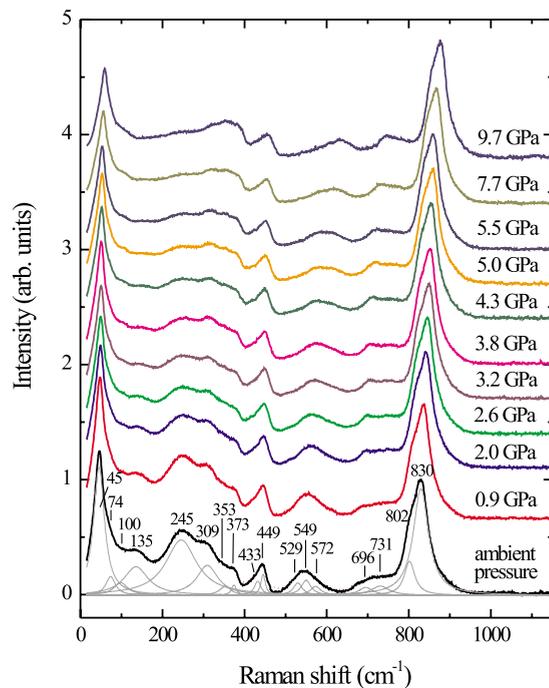

FIG. 4. (Color online) Raman spectra measured at different pressures. The fitting Lorentzians (gray thin lines) of the experimental spectrum measured at ambient pressure are also included in the plot; the resultant spectrum profile matches very well the experimental spectrum.

metrical stretching vibrations of the BO_6 octahedra and give rise to the peaks near 830 and 802 cm^{-1}. One F_{2g} mode is associated with internal BO_6 symmetrical bending vibrations and generates the Raman scattering near 549 cm^{-1} while the other F_{2g} mode consists of Pb vibrations (Pb-localized mode) and results in the Raman peak near 45 cm^{-1}. The remainder of the Raman-scattering signals observed at ambient pressure originate from ferroic nanoregions, which are assumed to have local rhombohedral-like symmetry because the low-temperature phases of relaxors that exhibit a normal para-to-ferroelectric phase transition are rhombohedral.[31,32] Thus, the peaks near 74 and 529 cm^{-1} are due to the rhombohedral splitting of the cubic F_{2g} modes. The Raman signals near 700, 433, and 135 cm^{-1} arise from rhombohedral modes corresponding in frequency to longitudinal infrared-active F_{1u} cubic modes of the prototype structure and they are, respectively, related to octahedral antisymmetrical stretching, octahedral antisymmetrical bending, and BO_3 translations against Pb atomic vector displacements. The peak near 575 cm^{-1} most probably results from a rhombohedral antisymmetrical stretching mode corresponding in frequency to the analogous transverse F_{1u} cubic mode, as revealed by far-infrared optical conductivity spectra.[33] The Raman peak near 245 cm^{-1} is

related to the cubic F_{1u} mode comprising B-site cation vibrations (B-cation localized mode), whose Raman activity is due to the existence of off-centered B cations in polar nanoregions. The Raman scattering near 300 and 353 cm^{-1} arises from Pb-O bond-stretching vibrations corresponding to a silent cubic mode; the Raman activity is caused by noncoplanar Pb shifts with respect to O atoms in {111} planes and the higher wave-number signal near 353 cm^{-1} is indicative of correlated off-shifts of Pb atoms. This peak assignment is applicable for $Pb(B',B'')O_3$ structures. The incorporation of Ba leads to additional Raman peaks. The signal near 100 cm^{-1}, which is well resolved in cross-polarized spectra,[3] is due to the presence of a second A-site cation. The peak near 373 cm^{-1} is due to shortened Pb-O bonds next to BaO_{12} polyhedra within {111} planes (see Fig. 5) while the signals near 449 and 731 cm^{-1} result from internal modes of deformed BO_6 octahedra adjoining BaO_{12} polyhedra along $\langle 111 \rangle$ directions (see Fig. 5). Hence, it is clear that the dilution of the Pb system with Ba leads to considerable local internal stress fields in the structure, which can oppose the effect of external pressure. Indeed, in the case of PST a soft mode appears at the critical pressure $p_c = 1.9$ GPa, whereas an additional lowest wave-number Raman peak at high pressures was not detected for PST-Ba, most probably due to the relatively small size and/or abundance of ferroic species with coherent atomic shifts distributed within the nonferroic matrix. However, the wave number of the Pb-localized mode near 45 cm^{-1} as a function of pressure has a kink near 4 GPa [see Fig. 6(a)], which corresponds to the stiffening of the structure as indicated by the start of the positive trend in the
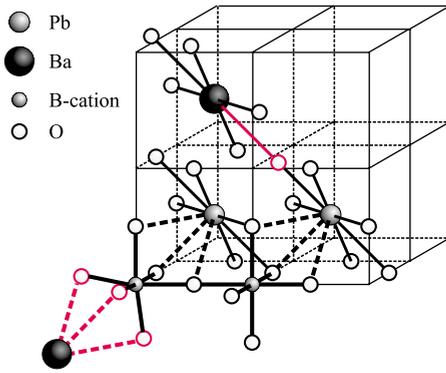
FIG. 5. (Color online) Representative structural species in a perovskite-type structure with a second A-site cation having an ionic radius larger than that of the prevalent A-site cation, which is the case of $(Pb_{1-x}Ba_x)BO_3$; Ba^{2+} has a larger ionic radius than that of Pb^{2+} and thus deforms the adjacent BO_6 octahedra along $\langle 111 \rangle$ directions and shortens the Pb-O bonds within $\{111\}$ planes.

$F(f)$ plot [Fig. 1(b)]. In addition, the wave number of the BO_3-Pb translation mode in ferroic regions substantially increases above 4 GPa [Fig. 6(b)], similarly to the behavior of the corresponding peak in PST near the critical pressure.[14] The high-pressure Raman spectra reveal two types of pressure-induced local structural changes that occur in both PST and PST-Ba: the suppression of off-centered shifts of B cations, as revealed by the intensity decrease in the Raman peak near 245 cm^{-1}, and the enhancement of coherent distorted PbO_{12} polyhedra, that results in the increase in intensity of the Raman scattering near 350–370 cm^{-1} (see Figs. 4 and 7). High-pressure Raman spectroscopic data on other
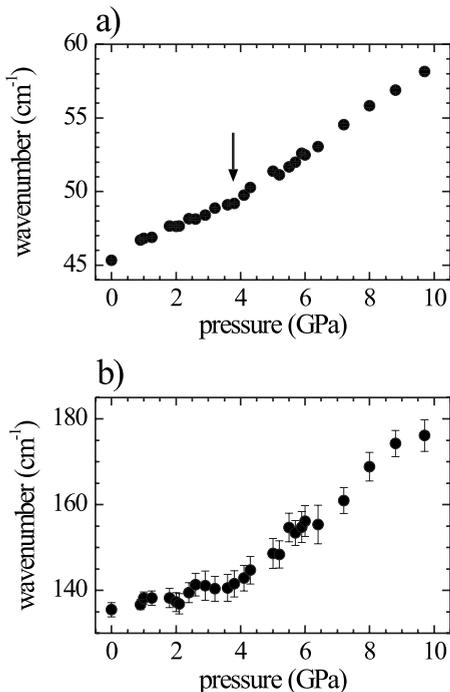

FIG. 6. (a) Pressure evolution of the position of Raman scattering generated by the Pb-localized mode and (b) that generated by the BO_3-Pb translational mode in ferroic nanoregions.
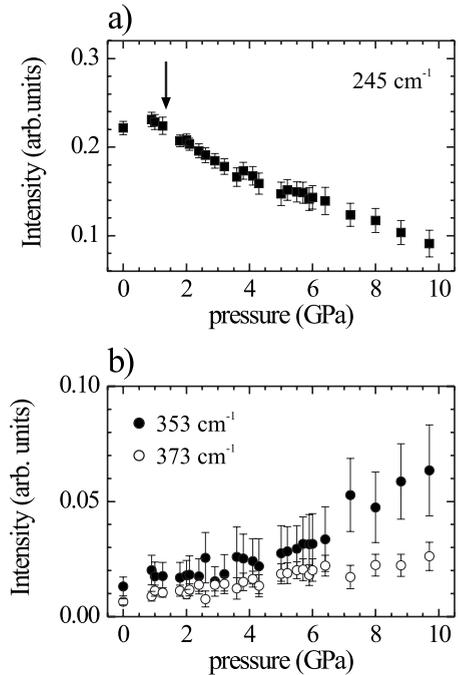

FIG. 7. (a) Pressure dependence of the integrated intensity of the anomalous Raman scattering near 245 cm^{-1} arising from B cations that are off-center shifted from their cubic positions and (b) the intensities of the anomalous Raman signals near 353 and 373 cm^{-1} generated from Pb-O bond-stretching vibrations of Pb-O ferroic species consisting of correlated off-shifts of Pb atoms with respect to oxygen atoms.

compounds[5,6,8–10,12,16] indicate that these structural changes are common for all Pb-based perovskite-type relaxors. In PST-Ba the off-centered B-site cations start to move toward their cubic positions at relatively low pressure, ~ 1.4 GPa [Fig. 7(a)], which is close to the characteristic feature near 2 GPa in the f-F plot, at which the plateaulike minimum of $F(f)$ begins [Fig. 1(b)]. This is similar to the case of pure PST, showing a drop in the corresponding Raman intensity near 1.5 GPa and a phase transition at 1.9 GPa. However, for PST-Ba the Raman intensity at 245 cm^{-1} gradually decreases up to the highest pressure reached in our experiment, whereas for PST the intensity drop is in a pressure range of approximately 1 GPa around the phase transition and above 2.5 GPa the intensity of the 245 cm^{-1} peak is almost constant,[14] showing a saturation in the local structural changes. This indicates that the incorporation of Ba also influences the behavior of the B-cation system under pressure and considerably enlarges the pressure range of structural rearrangements of initially off-centered B cations. The intensity of the peaks near 353 and 373 cm^{-1} arising from Pb-O bond stretching in Pb-O-Pb and Pb-O-Ba linkages, respectively, also change gradually with pressure [Fig. 7(b)]. Although these Raman signals are not very well resolved and, consequently, the intensity uncertainties are relatively large, it can be clearly seen [Fig. 7(b)] that at high pressures the rate of enhancement of the peak near 353 cm^{-1} is stronger than the peak near 373 cm^{-1}. This again indicates that the presence of Ba slows down the development of coherent ferroic species under pressure. Thus, the pressure evolution of

the Raman spectra shows that the chemically induced local elastic fields associated with A-positioned Ba are responsible for the diffuseness of the pressure-induced phase transition in PST-Ba.

IV. SUMMARY AND CONCLUSION

The incorporation of large dopant cations such as Ba^{2+} into the A sites of a perovskite structure can, in principle, be accommodated by one of two mechanisms; either the structure is locally distorted around the dopant cations but the long-range structure and unit-cell parameters remain unchanged, or the strain fields around the dopant cations interact and the structure undergoes uniform expansion. In many solid solutions, low levels of doping are accommodated by local strains while uniform expansion occurs at higher levels of substitution.[34,35] The Raman spectra of PST-Ba that we have reported clearly indicate that the incorporation of Ba into the structure of PST results in abundant local distortions of the structure. On the other hand, the comparison between the unit-cell parameters of PST and PST-Ba reveal no significant expansion of the unit cell under doping; with 22% Ba substitution the unit-cell parameter expands from 8.1532(4) Å in PST to 8.1647(4) Å in PST-Ba, i.e., 0.1%. This contrasts with the 0.8% expansion one would expect on the basis of ionic radii (1.49 and 1.61 Å for 12-coordinate Pb^{2+} and Ba^{2+}, respectively) if the unit-cell parameters were controlled by the A-O bond lengths. Instead of overall expansion, the incorporation of Ba must therefore create local strains within the structure, and the development of long-range ferroic order in this material is thus delayed to higher pressures compared to pure PST.

The existence of local structural distortions in the vicinity of A-positioned Ba cations, namely, distortion of BO_6 octahedra adjoining Ba along $\langle 111 \rangle$ and shortening of Pb-O bonds within $\{111\}$ planes, also explains why the sharp pressure-induced phase transition in PST becomes "diffuse" and spreads out over a pressure range in PST-Ba. Such smearing out of the transition cannot be explained within the context of a homogeneous order parameter[36,37] but reflects the local chemical inhomogeneities on the A sites and subsequent structural variations. Local elastic strains induced by the incorporation of Ba^{2+} create local potential barriers, thus shifting the "local transition" pressures to higher values, which depend on the nanoscale spatial variation in the Ba/Pb ratio. At the same time, the full three-dimensional connectivity of the octahedral framework provides a long-range background mean field within which the local structure exists. As a result, the overall pressure-induced phase transition of the average structure of PST-Ba is smeared out between 2 and 4 GPa. Although the development of ferroic long-range order is substantially disturbed by the presence of Ba, the high-pressure structural state of PST-Ba (above 4 GPa) exhibits structural features which are similar to those of the high-pressure phase of PST: the off-centered displacements of B-site cations are strongly suppressed, while the coherence length of ferroic Pb-O species is enhanced.

The comparison between pressure- and temperature-induced[4] structural changes in PST and PST-Ba also reveals that the replacement of Pb^{2+} by Ba^{2+} has the same effect on the transformation processes in Pb-based perovskite-type relaxor ferroelectrics, no matter if the thermodynamic variable is temperature or pressure. In both cases, Ba doping hampers the development of ferroic long-range order. This highlights the importance of potential barriers associated with chemically induced local strains for the occurrence of a relaxor structural state.

*Corresponding author.

†boriana.mihailova@uni-hamburg.de

‡rangel@vt.edu

[1] J. F. Scott, Science **315**, 954 (2007).

[2] A. A. Bokov and Z.-G. Ye, J. Mater. Sci. **41**, 31 (2006).

[3] V. Marinova, B. Mihailova, T. Malcherek, C. Paulmann, C. Lengyel, L. Kovacs, M. Veleva, M. Gospodinov, B. Güttler, R. Stosch, and U. Bismayer, J. Phys.: Condens. Matter **18**, L385 (2006).

[4] B. Mihailova, B. Maier, C. Paulmann, T. Malcherek, J. Ihringer, M. Gospodinov, R. Stosch, B. Güttler, and U. Bismayer, Phys. Rev. B **77**, 174106 (2008).

[5] J. Kreisel, B. Dkhil, P. Bouvier, and J.-M. Kiat, Phys. Rev. B **65**, 172101 (2002).

[6] J. Rouquette, J. Haines, V. Bornand, M. Pintard, Ph. Papet, B. Bonnet, and F. A. Gorelli, Solid State Sci. **5**, 451 (2003).

[7] B. Chaabane, J. Kreisel, B. Dkhil, P. Bouvier, and M. Mezouar, Phys. Rev. Lett. **90**, 257601 (2003).

[8] B. Chaabane, J. Kreisel, P. Bouvier, G. Lucazeau, and B. Dkhil, Phys. Rev. B **70**, 134114 (2004).

[9] A. Sani, B. Noheda, I. A. Kornev, L. Bellaiche, P. Bouvier, and J. Kreisel, Phys. Rev. B **69**, 020105 (2004).

[10] M. Ahart, R. E. Cohen, V. Struzhkin, E. Gregoryanz, D. Rytz, S. A. Prosandeev, H.-K. Mao, and R. J. Hemley, Phys. Rev. B **71**, 144102 (2005).

[11] S. N. Gvasaliya, V. Pomjakushin, B. Roessili, Th. Strässle, S. Klotz, and S. G. Lushnikov, Phys. Rev. B **73**, 212102 (2006).

[12] P.-E. Janolin, B. Dkhil, P. Bouvier, J. Kreisel, and P. A. Thomas, Phys. Rev. B **73**, 094128 (2006).

[13] J. Rouquette, J. Haines, G. Fraysse, A. Al-Zein, V. Bornand,

M. Pintard, Ph. Papet, and S. Hull, Inorg. Chem. **47**, 9898 (2008).

[14] B. Mihailova, R. J. Angel, A.-M. Welsch, J. Zhao, J. Engel, C. Paulmann, M. Gospodinov, H. Ahsbahs, R. Stosch, B. Güttler, and U. Bismayer, Phys. Rev. Lett. **101**, 017602 (2008).

[15] G.-M. Rotaru, S. N. Gvasaliya, V. Pomjakushin, B. Roessli, Th. Strässle, S. G. Lushnikov, T. A. Shaplygina, and P. Günter, J. Phys.: Condens. Matter **20**, 104235 (2008).

[16] A.-M. Welsch, B. Mihailova, M. Gospodinov, R. Stosch, B. Güttler, and U. Bismayer, J. Phys.: Condens. Matter **21**, 235901 (2009).

[17] J. Kreisel, P. Bouvier, B. Dkhil, P. A. Thomas, A. M. Glazer, T. R. Welberry, B. Chaabane, and M. Mezouar, Phys. Rev. B **68**, 014113 (2003).

[18] J. Kreisel, P. Bouvier, M. Maglione, B. Dkhil, and A. Simon, Phys. Rev. B **69**, 092104 (2004).

[19] R. J. Angel, M. Bujak, J. Zhao, G. D. Gatta, and S. D. Jacobsen, J. Appl. Crystallogr. **40**, 26 (2007).

[20] H. King and L. W. Finger, J. Appl. Crystallogr. **12**, 374 (1979).

[21] R. J. Angel, D. R. Allan, R. Miletich, and R. W. Finger, J. Appl. Crystallogr. **30**, 461 (1997).

[22] R. Ralph and L. W. Finger, J. Appl. Crystallogr. **15**, 537 (1982).

[23] R. Miletich, D. R. Allan, and W. F. Kuhs, in *High-Pressure and High-Temperature Crystal Chemistry*, edited by R. M. Hazen and R. T. Downs (Mineralogical Society of America, Washington D.C., 2000), pp. 445–519.

[24] R. Boehler, Rev. Sci. Instrum. **77**, 115103 (2006).

[25] R. G. Munro, G. J. Piermarini, S. Block, and W. B. Holzapfel, J. Appl. Phys. **57**, 165 (1985).

[26] R. J. Angel, in *Reviews in Mineralogy & Geochemistry*, edited by R. M. Hazen and R. T. Downs (Mineralogical Society of America, Washington D.C., 2000), Vol. 41, Chap. 2, p.35.

[27] M. Pasciak, M. Wolcyrz, and A. Pietraszko, Phys. Rev. B **76**, 014117 (2007).

[28] T. R. Welberry and D. J. Goossens, J. Appl. Crystallogr. **41**, 606 (2008).

[29] B. Mihailova, U. Bismayer, B. Güttler, M. Gospodinov, and L. Konstantinov, J. Phys.: Condens. Matter **14**, 1091 (2002).

[30] B. Mihailova, M. Gospodinov, B. Güttler, R. Stosch, and U. Bismayer, J. Phys.: Condens. Matter **19**, 275205 (2007).

[31] C. Perrin, N. Menguy, E. Suard, Ch. Muller, C. Caranoni, and A. Stepanov, J. Phys.: Condens. Matter **12**, 7523 (2000).

[32] P. M. Woodward and K. Z. Baba-Kishi, J. Appl. Crystallogr. **35**, 233 (2002).

[33] B. Mihailova, U. Bismayer, B. Güttler, M. Gospodinov, A. Boris, C. Bernhard, and M. Arozo, Z. Kristallogr. **220**, 740 (2005).

[34] E. K. H. Salje, U. Bismayer, B. Wruck, and J. Hensler, Phase Transitions **35**, 61 (1991).

[35] E. K. H. Salje, Phys. Rep. **215**, 49 (1992).

[36] E. K. H. Salje, Phys. Chem. Miner. **14**, 181 (1987).

[37] R. J. Angel, Am. Mineral. **77**, 923 (1992).